


Neural network atomic potential to investigate the dislocation dynamics in bcc iron

Hideki Mori **Department of Mechanical Engineering, College of Industrial Technology, 1-27-1 Nishikoya, Amagasaki, Hyogo 661-0047, Japan*Taisuke Ozaki †*Institute for Solid State Physics, University of Tokyo, 5-1-5 Kashiwanoha, Kashiwa, Chiba 277-8581, Japan*

(Received 8 November 2019; revised manuscript received 1 March 2020; accepted 1 April 2020; published 24 April 2020)

To design the mechanical strength of body-centered-cubic (bcc) iron, clarifying the dislocation dynamics is very important. Using systematically constructed reference data based on density functional theory (DFT) calculations, we construct an atomic artificial neural network (ANN) potential to investigate the dislocation dynamics in bcc iron with the accuracy of DFT calculations. The bulk properties and defect formation energies predicted by the constructed ANN potential are in good agreement with the reference DFT calculations. The $a_0/2\langle 111 \rangle\{110\}$ screw dislocation core structure predicted by the ANN potential is compact and nondegenerate. The Peierls barrier predicted by the ANN potential is 35.3 meV per length of the Burgers vector. These results are consistent with the DFT results. Furthermore, not only the Peierls barrier, but also the two-dimensional energy profile of the screw dislocation core position predicted by the ANN potential are in excellent agreement with the DFT results. These results clearly demonstrate the reproducibility and transferability of the constructed ANN potential for investigating dislocation dynamics with the accuracy of the DFT. Combined with advanced atomistic techniques, the ANN potential will be highly useful for investigating the dislocation dynamics in bcc iron at finite temperatures.

DOI: [10.1103/PhysRevMaterials.4.040601](https://doi.org/10.1103/PhysRevMaterials.4.040601)

Iron is among the most useful structural materials in our daily life. To reduce the environmental loads resulting from manufacturing activities of humans, improving and designing the mechanical strength of iron is very important. In general, the dynamics of screw dislocations plays a critical role in the mechanical behavior of body-centered-cubic (bcc) iron at low temperature. Therefore, the structure and energetics of screw dislocation cores in bcc iron have been well studied using highly accurate density functional theory (DFT) calculations [1–5]. However, owing to the high computational cost of DFT calculations, the number of atoms that can be practically handled by DFT is limited to a few hundred. Therefore, it is not easy to directly investigate the dynamics of dislocations at a finite temperature via DFT calculations. On the other hand, molecular dynamics (MD) simulations on the scale of millions of atoms with empirically parametrized potentials enable more flexible modeling. In principle, however, the accuracy of these potentials is limited by their function type. Several types of potentials have been proposed, such as the embedded atom method (EAM), modified EAM, and Tersoff potential [6,7]. To the best of our knowledge, no potentials can reproduce the dislocation core structure and energetics of bcc iron with the accuracy of the DFT.

One strategy to directly investigate dislocation dynamics with DFT accuracy is to construct an atomic potential based

on an artificial neural network (ANN) framework [8,9]. By the universal approximation theorem, the ANN can compute any function with arbitrary accuracy [10]. Therefore, the interatomic potential based on an ANN (ANN potential) is expected to reproduce the potential energy surface (PES) of calculations using sufficient reference DFT data sets. Excellent applications to various materials have already been demonstrated, such as Si [11], Cu [12], and $\text{Li}_x\text{PO}_y\text{N}_z$ [13]. An ANN has also been shown to predict not only the total energy of a system but also the electronic density of states from reference DFT data sets [14]. Thus, the ANN potential is a sophisticated and promising tool for advanced materials design. Recently, an interatomic potential based on Gaussian process regression, known as the Gaussian approximation potential (GAP), was proposed for bcc iron [15]. The GAP has a highly flexible function form, same as the ANN. The bulk properties and defect formation energies predicted by the GAP are in excellent agreement with those from the reference DFT calculations. However, the reproducibility and transferability of the GAP for the energetics of the dislocation core are not sufficiently evaluated [15,16]. Furthermore, a discrepancy remains between the GAP and DFT regarding the dislocation core structure [17]. Therefore, in this work, we construct a new ANN potential for investigating the dislocation dynamics in bcc iron with the accuracy of DFT. To demonstrate the reproducibility and transferability of this ANN potential, we evaluate the $a_0/2\langle 111 \rangle\{110\}$ screw dislocation core structure and its energetics in detail. We also evaluate other nonscrew dislocation core structures, which play important roles in

*Corresponding author: morih@cit.sangitan.ac.jp

†t-ozaki@issp.u-tokyo.ac.jp

dislocation dynamics owing to the reactions between them, such as junction formation.

To construct an ANN potential for investigating the dislocation core structure, we use the ANN method proposed by Behler and Parrinello [8]. In this method, the output of the ANN is the atomic energy ϵ_i^{ANN} of the i th atom, and the total energy E^{ANN} of the target system is expressed as the contribution of the atomic energy:

$$E^{\text{ANN}} = \sum_{i=1}^N \epsilon_i^{\text{ANN}}[\mathbf{G}(\mathbf{R}_i)], \quad (1)$$

where N is the number of atoms in a target system; \mathbf{G} is the vector set of descriptors, which describes the local atomic environment around the i th atom; and \mathbf{R}_i represents the atomic position around the i th atom. The descriptor transforms the atomic positions around the i th atom to an adequate input vector set. To investigate the crystal structure, the descriptor is required to satisfy the translational, rotational, and permutation invariance of the atomic energy. We use the Chebyshev descriptors proposed by Artrith *et al.* [18]. In this method, the two-body radial contribution is described as

$$G_{\alpha}^{\text{pair}} = \sum_{j \neq i} T_{\alpha} \left(\frac{2r_{ij}}{R_c} - 1 \right) f_c(r_{ij}), \quad (2)$$

where r_{ij} is the atomic distance between atoms i and j , R_c is the cutoff radius, and T_{α} is the Chebyshev polynomial of the first kind [18]. The Chebyshev polynomials T_n are defined by a recurrence relation as

$$T_{n+1}(x) = 2xT_n(x) - T_{n-1}(x), \quad (3)$$

where $T_0(x)$ and $T_1(x)$ are 1 and x , respectively. Because of the introduction of the cutoff function $f_c(r_{ij})$, only atoms within the cutoff radius R_c are considered in the sum of Eq. (2), and the calculation cost remains $O(N)$. To smoothly truncate both the value and its first derivative, we use a cosine cutoff function defined as

$$f_c(r_{ij}) = \begin{cases} \frac{1}{2} \left[\cos \left(\frac{\pi r_{ij}}{R_c} \right) + 1 \right] & (r_{ij} \leq R_c) \\ 0 & (r_{ij} > R_c). \end{cases} \quad (4)$$

In this work, we use R_c at 0.65 nm. The three-body angle contribution is described as

$$G_{\alpha}^{\text{triple}} = \sum_{j \neq i, k \neq i, j} T_{\alpha} \left(\frac{1}{2} (\cos \theta_{ijk} + 1) \right) f_c(r_{ij}) f_c(r_{ik}), \quad (5)$$

where r_{ij} , r_{ik} , and r_{jk} are the atomic distances between atoms i , j , and k , and θ_{ijk} is the angle defined by the three atoms. We use 9 radial functions and 19 angular functions. Hence, the total dimension of the input vector set of descriptors is 28. We set ten neurons in each layer in the hidden layer of the ANN potential, and used a hyperbolic tangent with a linear twisting function as the activation function of the hidden layers [19]. To train the ANN potential, the cost function C is defined as follows:

$$C(\{\mathbf{w}, \mathbf{b}\}) = \frac{1}{2} \sum_{t=1}^{N_s} [E_t^{\text{ANN}}(\{\mathbf{w}, \mathbf{b}\}) - E_t^{\text{DFT}}]^2, \quad (6)$$

where N_s is the number of structures in the data set, and E_t^{ANN} and E_t^{DFT} are potential energies of the t th structure of the ANN potential and the DFT calculation, respectively. The matrix \mathbf{w} and vector \mathbf{b} are fitting parameter sets, termed the weight matrix and bias vector, respectively. Using $\frac{\partial C}{\partial \mathbf{w}}$ and $\frac{\partial C}{\partial \mathbf{b}}$ by the back-propagation technique [19], both the weight matrix and bias vector are optimized to minimize the cost function. To optimize the weight matrix and the bias vector, we use the limited memory Broyden-Fletcher-Goldfarb-Shanno method [20]. For the ANN potential training, we use the Atomic Energy Network (`ænet`) package by Artrith and Urban [9]. First, we consider 100 000 training steps to optimize the weight matrix and bias vector. We then check the phonon dispersion of bcc iron, defect formation energies, and relaxed atomic configurations of defects predicted by the ANN potential, applying the weight matrix and bias vector every 10,000 steps. In the training procedure, information on the force (gradient of potential energy) is not used. Therefore, the above protocol may be suitable for checking overfitting. We found that the weight matrix and bias vector at the 50 000th step are best fits.

The QUANTUM ESPRESSO package [21] was used to construct the reference DFT structure energy data sets for iron. We generate two types of data sets for the reference DFT dataset: an ideal crystal structure dataset and a perturbed structure dataset. The bcc, face-centered-cubic (fcc), hexagonal-close-packed (hcp), and simple cubic structures are chosen as the ideal crystal structures. We calculate the potential energy at the equilibrium unit cell and the potential energies for systematically transformed unit cells. To cover enough area of the reference PES, the perturbed structures are generated by random displacement of the atomic positions to the initial structures in the range of $\pm 0.05a_0$. We choose the bulk bcc, point defects, and surface structures to define the initial structures. As point defect structures, we define the vacancy, divacancy, and self-interstitial structures. As self-interstitial structures, the tetrahedral (T) -site, octahedral (O) -site, [100]-dumbbell, [110]-dumbbell, and [111]-dumbbell configurations are chosen. The (100), (110), (111), and (112) surfaces are chosen as the surface structures. The energy surface for the sliding of two adjacent atomic blocks in a two-dimensional (2D) space, known as the generalized stacking fault (GSF) energy surface, plays a critical role in determining the dislocation core structure [2, 15, 22]. The (110) and (112) planes, which are the most important slip planes of bcc iron, are chosen as the GSF energy surface model. We prepared 5751 atomic structure energy data sets of iron [23]. The bulk properties and defect formation energies predicted by the constructed ANN potential are in excellent agreement with those from the reference DFT calculation [23]. Thus, the constructed ANN potential is expected to be a highly accurate replica potential of the DFT.

Now, by using the constructed ANN potential, we evaluate the $a_0/2\langle 111 \rangle\{110\}$ screw dislocation core structure and its energetics in bcc iron. For large-scale atomic modeling, we modify the potential driver of `ænet` as a module in LAMMPS [25]. We use the $22[11\bar{2}] \times 38[1\bar{1}0] \times 1/2[111]$ bcc bulk model, which is only periodic along the [111] direction. The total number of atoms in the model is 5016. To create the

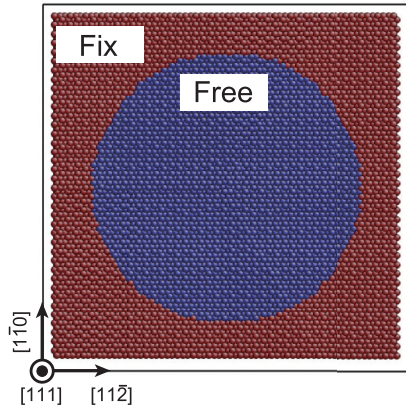


FIG. 1. Schematic of bulk bcc model for creating the dislocation core.

dislocation core structure at the center of the (111) plane of the model, we apply to all the atoms the anisotropic elastic solution of the displacement field. Subsequently, we optimize the atomic position of the model except for the atoms, which are located more than 6 nm away from the dislocation core, as shown in Fig. 1. The criterion for optimization is set as 0.05 eV/nm for the subsequent calculations. Figure 2 shows the atomic configuration of the screw dislocation core in a stable state, known as the easy core, with the differential displacement (DD) map [26]. We define the position of the easy core as the centroid of three triangularly positioned atoms indicated by the blue cross in Fig. 2 [1–3]. The core structure predicted by the ANN potential has a compact and nondegenerate structure. These results are in agreement with previous DFT calculations [1,3–5]. We define the relative position ($P_{[11\bar{2}]}, P_{[1\bar{1}0]}$) of the dislocation core from the easy core in the (111) plane as

$$P_{[11\bar{2}]} = \frac{2\sqrt{3}}{3}(d_{[111]}^2 + d_{[111]}^3 - 2d_{[111]}^1),$$

$$P_{[1\bar{1}0]} = \frac{2\sqrt{6}}{3}(d_{[111]}^2 - d_{[111]}^3), \quad (7)$$

where $d_{[111]}^i$ is the relative displacement of the atomic position from the atomic position of the reference bulk model along the [111] direction, and $i = 1, 2, 3$ indicate the atomic numbering in Fig. 1 [1,3–5]. To control the position of these three atoms,

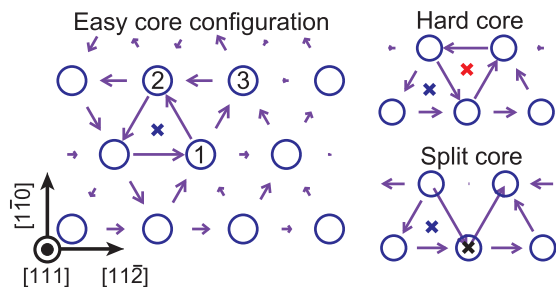


FIG. 2. Atomic configurations of the screw dislocation core with the differential displacement (DD) map. Blue, red, and black crosses indicate the positions of the easy core, hard core, and split core, respectively. See text for details of the atomic numbering.

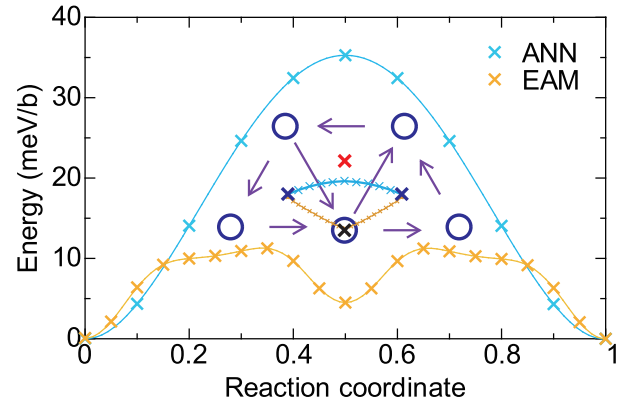


FIG. 3. Peierls potential and migration path of dislocation core (inset) along the reaction coordinate predicted by the ANN (sky blue) potential and EAM (yellow) potential [24]. Blue, red, and black crosses indicate the positions of the easy core, hard core, and split core, respectively.

we can set the dislocation core at arbitrary positions. In Fig. 2, we show the two important dislocation core positions, known as the hard core and split core, and the DD map. We evaluate the Peierls barrier, which is the activation enthalpy of dislocations to migrate from one easy core position to another adjacent easy core position [3–5,27]. Using the nudged elastic band method [28,29], we calculate the energy profile along the reaction coordinate, known as the Peierls potential. The corresponding results are shown in Fig. 3. For reference, by using the EAM potential [24], the Peierls potential is also calculated, as shown in Fig. 3. The Peierls potential predicted by the ANN potential is a single hump type. Thus, from the value of the local maximum, the Peierls barrier is evaluated as 35.3 meV/b, where b is the length of the Burgers vector [$b = (\sqrt{3}/2)a_0$]. Using Eq. (7), the minimum energy migration path of the screw dislocation core is calculated, as shown in Fig. 3. The sky-blue line and yellow line indicate the migration paths predicted by the ANN and EAM potentials, respectively. The path predicted by the ANN potential is curved when approaching the hard core position, represented by the red cross [3–5]. The DD map superimposed on the path shows the transition state predicted by the ANN potential. These results are in agreement with previous DFT calculations [1,3–5]. On the other hand, the Peierls potential predicted by the EAM potential is of the double hump type, and the evaluated Peierls barrier is 11.3 meV/b. The migration path predicted by the EAM potential is widely curved so that it is close to the split core position, denoted by the black cross. To evaluate the reproducibility and transferability of the ANN potential for investigating the dislocation dynamics, we calculate the potential energy profile as a function of the screw dislocation core position, termed the 2D Peierls potential. The 2D Peierls potential not only determines the Peierls barrier and migration path of the dislocation core, but also controls the energetics of double kink formation, which plays an important role in the mobility of the screw dislocation at a finite temperature [30,31]. For the threefold symmetry of the bcc lattice, the 2D Peierls potentials are characterized by the energy profile along the cross-sectional line between the

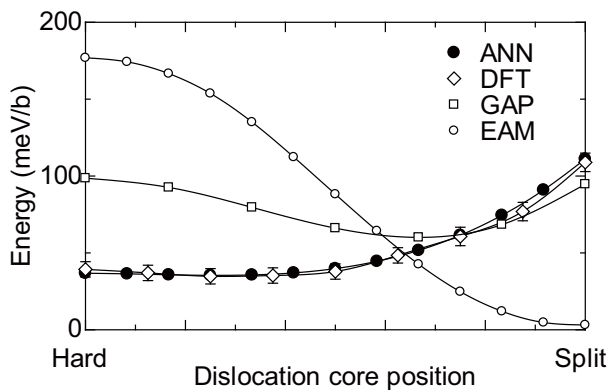


FIG. 4. Energy profile along the cross-sectional line between the hard core and split core positions predicted by the ANN and EAM potentials [24] and the GAP [15] with reference DFT calculations from Ref. [3].

core and split core positions [3–5]. Figure 4 shows the energy profile predicted by the ANN potential along with the previous DFT calculations from Ref. [3]. For reference, by using the GAP [15] and EAM [24], the energy profiles are calculated and displayed in Fig. 4. The Peierls potentials at the hard core and split core positions are 36.7 and 111.1 meV/b, respectively. The energy profiles predicted by the ANN potential are in excellent agreement with those from the previous DFT calculations [3–5]. On the other hand, the Peierls potentials predicted by the EAM potential decrease with the shift from a hard core to a split core, from 176.9 to 3.1 meV/b at the hard core and split core positions, respectively. This result is a general trend in the EAM potentials. The Peierls potentials at the hard core and split core positions predicted by the GAP are 98.6 and 94.7 meV/b, respectively. Compared with DFT results, the local minimum of the energy profile predicted by the GAP widely shifts to the split core and is 60.1 meV/b, which is almost the same as the Peierls barrier predicted by the GAP in a previous study (64 meV/b) [15]. We emphasize that the constructed ANN potential is the first interatomic potential which correctly predicts the energy profile between the hard core and the split core with the accuracy of the DFT without electronic state evaluation. We also directly calculate the formation energy for the double kink pair nucleation of screw dislocations in bcc iron using the ANN potential. We use the $22[11\bar{2}] \times 38[1\bar{1}0] \times 30[111]$ bcc bulk model. The total number of atoms in the model is 300 960. First, we make a straight screw dislocation using the same procedure as shown in Fig. 1. Then, to create a double kink pair, we shift the dislocation cores in the middle $30b$ layer to the next adjacent easy core position along the $[11\bar{2}]$ direction and optimize the atomic configuration of the model. The formation energy for the nucleation of the double kink pair is 0.94 eV, which is consistent with the estimated values from the line tension model based on the DFT dataset: 0.73–0.86 eV [3,32].

Lastly, we evaluate other nonscrew dislocation core structures to check the reproducibility and transferability of the ANN potential in detail. Recently, via DFT calculations, Fellingner *et al.* determined four nonscrew dislocation core structures, $a_0/2\langle 111 \rangle\{110\}$ edge, $a_0/2\langle 111 \rangle\{110\}$ 71° mixed,

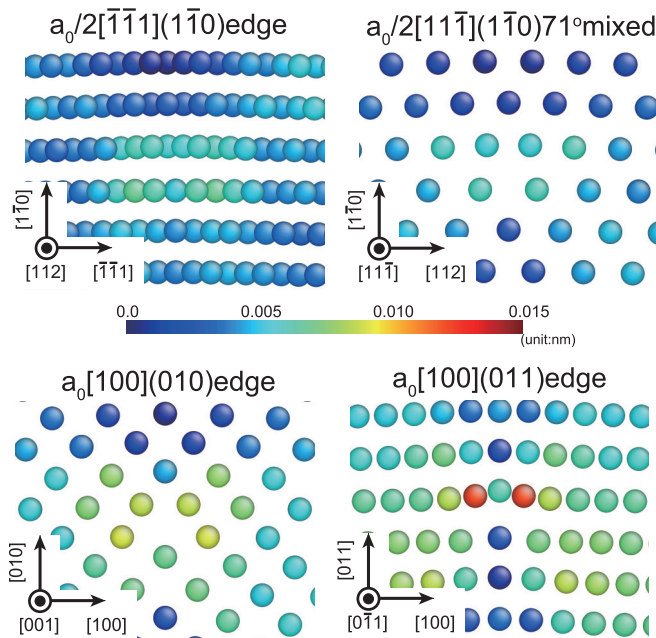


FIG. 5. Atomic configuration of $a_0/2\langle 111 \rangle\{110\}$ edge, $a_0/2\langle 111 \rangle\{110\}$ 71° mixed, $a_0\langle 100 \rangle\{110\}$ edge, and $a_0\langle 100 \rangle\{100\}$ edge dislocations predicted by the ANN potential. The atomic coloring and map show the error norm from the DFT results in Ref. [17]. See text for details.

$a_0\langle 100 \rangle\{110\}$ edge, and $a_0\langle 100 \rangle\{100\}$ edge dislocations [17]. Not only their dynamics, but also the reactions between them play important roles in the mechanical behavior of bcc iron. These results also verified the accuracy and predictive ability of various interatomic potentials including the GAP. They show that the GAP fails to reproduce the $a_0\langle 100 \rangle\{110\}$ edge dislocation core structure. The atomic configurations of these dislocation cores predicted by the ANN potential are shown in Fig. 5. The atomic coloring and map indicate the error norm of the atomic positions between results from the ANN potential and DFT. We calculate the error norm e_i of individual atoms as

$$e_i = \sqrt{|\mathbf{r}_i^{\text{ANN}} - \mathbf{r}_i^{\text{DFT}}|^2}, \quad (8)$$

where $\mathbf{r}_i^{\text{ANN}}$ is the position of the i th atom predicted by the ANN potential, and $\mathbf{r}_i^{\text{DFT}}$ is the position of the corresponding atom from the DFT results. We consider the DFT atomic configuration of the dislocation core and initial input configuration to calculate the ANN potential from the available data in Ref. [17]. All error norms are less than 0.015 nm. Several error norms in the $a_0\langle 100 \rangle\{110\}$ edge dislocation core are slightly larger than others. However, the core structure is still consistent with the DFT results. These results clearly demonstrate the excellent reproducibility and transferability of the constructed ANN potential. Note that the difference in the predicted dislocation core structure and energetics between the ANN potential and the GAP may arise from the difference in the method for constructing the reference DFT data. To cover enough area of the reference PES, we add random displacements to the initial structures and sampled each atomic configuration and total energy as reference data

sets. On the other hand, to cover enough area of the reference PES for the reference DFT data of the GAP, Dragoni *et al.* performed MD simulations at various temperatures [15], and sampled each atomic configuration and total energy as reference data sets. The sampling by random displacements might be more efficient than the sampling by MD simulation.

In summary, we construct an atomic ANN potential to investigate the dislocation dynamics in bcc iron. The bulk properties and defect formation energies predicted by the constructed ANN potential are in good agreement with those from the reference DFT calculations. The $a_0/2\langle 111 \rangle\{110\}$ screw dislocation core structure and its energetics as well as the nonscrew dislocation core structure, both predicted by the ANN potential, are in excellent agreement with those from the DFT calculations; this confirms the excellent reproducibility and transferability of the constructed ANN potential. By using MD simulation techniques, the constructed ANN potential enables the large-scale direct investigation of dislocation dynamics with the accuracy of the DFT. Furthermore, combined with advanced atomistic techniques, such as strain-boost hyperdynamics [33], diffusive molecular dynamics [34], and

ring-polymer molecular dynamics [35], the ANN potential will be vital in investigating the dislocation dynamics in bcc iron at finite temperatures. The computational time of the ANN potential is approximately 5 ms/atom, which is approximately 100 times longer than that of the EAM potentials. However, recent progress in high-performance computing might overcome this disadvantage soon. There is no limitation on the descriptor type of the ANN potential. Hence, not only the local atomic coordinates but also other physical quantities can be adopted as input parameters. Our future work will focus on constructing a new ANN potential integrated with spin dynamics to investigate the magnetic effect in the phase stability and dislocation mobility of iron at high temperatures.

The ANN potential module implemented in LAMMPS, modified `ænet` for the LAMMPS library, and parameter file of iron are freely available online [36].

This work was partly supported by the Priority Issue (creation of new functional devices and high-performance materials to support next-generation industries) using Post “K” Computer, MEXT, Japan.

-
- [1] L. Ventelon and F. Willaime, *J. Comput.-Aided. Mater. Des.* **14**, 85 (2007).
- [2] L. Ventelon and F. Willaime, *Philos. Mag.* **90**, 1063 (2010).
- [3] M. Itakura, H. Kaburaki, and M. Yamaguchi, *Acta Mater.* **60**, 3698 (2012).
- [4] L. Ventelon, F. Willaime, E. Clouet, and D. Rodney, *Acta Mater.* **61**, 3973 (2013).
- [5] L. Dezerald, L. Ventelon, E. Clouet, C. Denoual, D. Rodney, and F. Willaime, *Phys. Rev. B* **89**, 024104 (2014).
- [6] J. J. Möller and E. Bitzek, *Modell. Simul. Mater. Sci. Eng.* **22**, 045002 (2014).
- [7] J. J. Möller, M. Mrovec, I. Bleskov, J. Neugebauer, T. Hammerschmidt, R. Drautz, C. Elsässer, T. Hickel, and E. Bitzek, *Phys. Rev. Mater.* **2**, 093606 (2018).
- [8] J. Behler and M. Parrinello, *Phys. Rev. Lett.* **98**, 146401 (2007).
- [9] N. Artrith and A. Urban, *Comput. Mater. Sci.* **114**, 135 (2016).
- [10] G. Cybenko, *Math. Control Signal Syst.* **2**, 303 (1989).
- [11] J. Behler, R. Martoňák, D. Donadio, and M. Parrinello, *Phys. Rev. Lett.* **100**, 185501 (2008).
- [12] N. Artrith and J. Behler, *Phys. Rev. B* **85**, 045439 (2012).
- [13] V. Lacivita, N. Artrith, and G. Ceder, *Chem. Mater.* **30**, 7077 (2018).
- [14] Y. Umeno and A. Kubo, *Comput. Mater. Sci.* **168**, 164 (2019).
- [15] D. Dragoni, T. D. Daff, G. Csányi, and N. Marzari, *Phys. Rev. Mater.* **2**, 013808 (2018).
- [16] F. Maresca, D. Dragoni, G. Csányi, N. Marzari, and W. A. Curtin, *npj Comput. Mater.* **4**, 69 (2018).
- [17] M. R. Fellinger, Anne Marie Z. Tan, L. G. Hector, Jr., and D. R. Trinkle, *Phys. Rev. Mater.* **2**, 113605 (2018).
- [18] N. Artrith, A. Urban, and G. Ceder, *Phys. Rev. B* **96**, 014112 (2017).
- [19] Y. A. LeCun, L. Bottou, G. B. Orr, and K.-R. Müller, in *Neural Networks: Tricks of the Trade* (Springer, New York, 2012), pp. 9–48.
- [20] R. H. Byrd, P. Lu, J. Nocedal, and C. Zhu, *SIAM J. Sci. Comput.* **16**, 1190 (1995).
- [21] P. Giannozzi, S. Baroni, N. Bonini, M. Calandra, R. Car, C. Cavazzoni, D. Ceresoli, G. L. Chiarotti, M. Cococcioni, I. Dabo *et al.*, *J. Phys.: Condens. Matter* **21**, 395502 (2009).
- [22] V. Vitek, *Philos. Mag.* **18**, 773 (1968).
- [23] See Supplemental Material at <http://link.aps.org/supplemental/10.1103/PhysRevMaterials.4.040601> for details of the construction of reference DFT data and bulk properties, defect formation energies, and surface energies predicted by the constructed ANN potential.
- [24] M. Mendeleev, S. Han, D. Srolovitz, G. Ackland, D. Sun, and M. Asta, *Philos. Mag.* **83**, 3977 (2003).
- [25] S. Plimpton, *J. Comput. Phys.* **117**, 1 (1995).
- [26] V. Vitek, R. Perrin, and D. Bowen, *Philos. Mag.* **21**, 1049 (1970).
- [27] R. Gröger and V. Vitek, *Modell. Simul. Mater. Sci. Eng.* **20**, 035019 (2012).
- [28] G. Henkelman, B. P. Uberuaga, and H. Jónsson, *J. Chem. Phys.* **113**, 9901 (2000).
- [29] G. Henkelman and H. Jónsson, *J. Chem. Phys.* **113**, 9978 (2000).
- [30] K. Edagawa, T. Suzuki, and S. Takeuchi, *Mater. Sci. Eng. A* **234**, 1103 (1997).
- [31] K. Edagawa, T. Suzuki, and S. Takeuchi, *Phys. Rev. B* **55**, 6180 (1997).
- [32] L. Proville, L. Ventelon, and D. Rodney, *Phys. Rev. B* **87**, 144106 (2013).
- [33] S. Hara and J. Li, *Phys. Rev. B* **82**, 184114 (2010).
- [34] J. Li, S. Sarkar, W. T. Cox, T. J. Lenosky, E. Bitzek, and Y. Wang, *Phys. Rev. B* **84**, 054103 (2011).
- [35] R. Freitas, M. Asta, and V. V. Bulatov, *npj Comput. Mater.* **4**, 55 (2018).
- [36] <https://github.com/HidekiMori-CIT/aenet-lammps>